Article

Co-Fe-Si Aerogel Catalytic Honeycombs for Low Temperature Ethanol Steam Reforming

Montserrat Domínguez [1,2], Elena Taboada [1], Elies Molins [3] and Jordi Llorca [1,2,]*

[1] Institute of Energy Technologies, Universitat Politècnica de Catalunya, Diagonal 647, Ed. ETSEIB, 08028 Barcelona, Spain; E-Mails: montserrat.dominguez.escalante@upc.edu (M.D.); elena.taboada@upc.edu (E.T.)

[2] Centre for Research in Nanoengineering, Universitat Politècnica de Catalunya, Pasqual i Vila 15, 08028 Barcelona, Spain

[3] Institut de Ciència de Materials de Barcelona, Consejo Superior de Investigaciones Científicas, Campus de la UAB, 08193 Bellaterra, Spain; E-Mail: elies.molins@icmab.es

* Author to whom correspondence should be addressed; E-Mail: jordi.llorca@upc.edu; Tel.: +34-93-4011708; Fax: +34-93-4017149.

Abstract: Cobalt talc doped with iron (Fe/Co~0.1) and dispersed in SiO_2 aerogel was prepared from silica alcogel impregnated with metal nitrates by supercritical drying. Catalytic honeycombs were prepared following the same procedure, with the alcogel synthesized directly over cordierite honeycomb pieces. The composite aerogel catalyst was characterized by X-ray diffraction, scanning electron microscopy, focus ion beam, specific surface area and X-ray photoelectron spectroscopy. The catalytic layer is about 8 μm thick and adheres well to the cordierite support. It is constituted of talc layers of about 1.5 μm × 300 nm × 50 nm which are well dispersed and anchored in a SiO_2 aerogel matrix with excellent mass-transfer properties. The catalyst was tested in the ethanol steam reforming reaction, aimed at producing hydrogen for on-board, on-demand applications at moderate temperature (573–673 K) and pressure (1–7 bar). Compared to non-promoted cobalt talc, the catalyst doped with iron produces less methane as byproduct, which can only be reformed at high temperature, thereby resulting in higher hydrogen yields. At 673 K and 2 bar, 1.04 $NL_{H2} \cdot mL_{EtOH(l)}^{-1} \cdot min^{-1}$ are obtained at S/C = 3 and W/F = 390 $g \cdot min \cdot mol_{EtOH}^{-1}$.
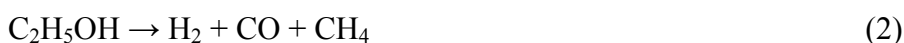
---

1. Introduction

The development of proton exchange membrane fuel cells (PEMFC) for the market of power sources for portable and mobile applications has moved researchers to investigate the development of small scale catalytic fuel reformers for on-site hydrogen generation from various liquid fuels as an alternative to direct hydrogen storage [1,2]. Among liquid fuels that are currently considered, ethanol is particularly appealing since it is a renewable source when obtained from biomass; it is easy to handle and distribute and it is readily available [3]. One of the most important drawbacks of current catalytic reformers is the lack of fast start up and rapid response to varying loads. In this context, aerogel-based catalysts may play a significant role since their mass transfer characteristics are excellent and offer new possibilities for conducting reforming reactions.

Many studies have been focused on ethanol steam reforming (ESR) using supported nickel, cobalt and noble metal catalysts aimed at generation of hydrogen [4–6] (Equation 1).

$$C_2H_5OH + 3H_2O \rightarrow 6H_2 + 2CO_2 \tag{1}$$

An efficient catalyst for hydrogen production from ethanol has to dissociate the C-C bond, maintain a low CO concentration and be stable under catalytic operation. A survey of the literature reveals that noble metal-based catalysts perform well for ESR [7–9]. They are stable and exhibit high activity, but only at high temperature (>800 K). The reason is that the reaction mechanism involves the decomposition of ethanol at moderate temperature into a mixture of hydrogen, carbon monoxide and methane (Equation 2), followed by the water gas shift reaction (WGS, Equation 3) and, finally, the steam reforming of methane at high temperature (Equation 4). The reaction mechanism over nickel-based catalysts follows the same steps as over noble metal-based catalysts; however, the particles of nickel species tend to sinter under ESR reaction conditions.

$$C_2H_5OH \rightarrow H_2 + CO + CH_4 \tag{2}$$

$$CO + H_2O \rightarrow H_2 + CO_2 \tag{3}$$

$$CH_4 + 2\,H_2O \rightarrow 4\,H_2 + CO_2 \tag{4}$$

In contrast, cobalt-based catalysts can operate at a much lower temperature, typically at 673–823 K, since they do not yield methane as an intermediate species in the reaction mechanism, which can only be reformed at high temperature [10–38]. Over cobalt-based catalysts, ethanol is first dehydrogenated at low temperature into a mixture of hydrogen and acetaldehyde (Equation 5), and then acetaldehyde reacts with steam to yield mainly hydrogen and carbon oxides (Equation 6), which participate in the WGS (Equation 3), or decompose into carbon monoxide and methane (Equation 7):

$$C_2H_5OH \rightarrow H_2 + CH_3CHO \tag{5}$$

$$CH_3CHO + H_2O \rightarrow 3\ H_2 + 2\ CO \tag{6}$$

$$CH_3CHO \rightarrow CH_4 + CO \tag{7}$$

Recently, we reported that cobalt talc ($Co_3[Si_2O_5]_2(OH)_2$) in a SiO_2 aerogel host is an active and selective catalyst to carry out ESR even at a lower temperature [39,40]. At 623 K, a reformate composition of 68.7% H_2, 23.2% CO_2, 1.0% CO and 7.1% CH_4 is found at a steam-to-carbon ratio of S/C = 1.5 (stoichiometric ethanol-water mixture, Equation 1) and full ethanol conversion [39]. In addition, the catalyst exhibits fast start-up (few seconds) and a stable reformate composition is obtained, even after shut-down and exposure to air up to 613 K. High resolution transmission electron microscopy, X-ray diffraction, magnetic measurements and in situ X-ray photoelectron spectroscopy experiments [41] have revealed that cobalt talc undergoes delamination into individual nanolayers under reaction conditions that remain fixed in the aerogel host. Simultaneously, metal cobalt ensembles segregate at the surface of the nanolayers facilitating the redox pair $Co^0 \leftrightarrow Co^{2+}$, thus offering a composite material with high surface area and reactivity, accounting for the outstanding catalytic behavior observed. This catalyst has been also tested in a catalytic membrane reactor for ESR with even faster response to varying loads [42].

On the other hand, it has been demonstrated that alloying cobalt with more electronegative elements such as Ni or Cu results in worse catalytic performance in terms of hydrogen yield, whereas alloying cobalt with the less electronegative elements Fe [22,43,44] and Mn [35,37] promotes the redox pair $Co^0 \leftrightarrow Co^{2+}$, both in terms of a lower cobalt reduction temperature as well as a fast re-oxidation, which in turn results in a better catalytic stability. An important advantage of conducting the ESR at low temperature is that the WGS equilibrium favors the formation of hydrogen and CO_2 at the expense of CO and water (Equation 3), thus maximizing the production of H_2 and avoiding the requirement of additional WGS units at the reactor outlet. This condition considerably simplifies the fuel processor design, both in terms of number of catalytic stages required as well as heat transfer management. Also, the addition of Fe and Mn promoters hinders acetaldehyde decomposition (Equation 7) and less methane is formed as byproduct. In this work, we have extended our work on cobalt talc ($Co_3[Si_2O_5]_2(OH)_2$) in SiO_2 aerogel host by studying the effect of Fe addition on the catalytic performance for ESR under practical conditions. To that end, we have tested honeycomb structures loaded with the aerogel catalyst under different operational conditions.

2. Results and Discussion

2.1. Catalysts Characterization

The surface area measured for both powdered catalysts is about 330 $m^2 \cdot g^{-1}$, and the average Barrett-Joyner-Halenda (BJH) pore size is 9.2 nm. These values are characteristic of aerogel structures [41]. The XRD profile of the powdered *aer-CoFeSi* catalyst is shown in Figure 1, along with that of *aer-CoSi* [41] for comparison. Both profiles are similar and show diffraction peaks characteristic of the talc structure [45]. The talc structure corresponds to a layered metal silicate hydroxide, $(Co,Fe)_3[Si_2O_5]_2(OH)_2$, which is synthesized under supercritical drying between SiO_2 and the metal precursors [41]. The peak measured at low angles corresponds to the basal plane (001) of the layered

structure. This peak exhibits a very low intensity, which means that the number of layers in the talc crystallites is low, consistent with a good dispersion of the catalyst particles in the aerogel host. The atomic ratio Co:Fe:Si measured by X-ray fluorescence (XRF) is 0.31:0.04:1. The amount of metal added is similar to that observed in the sample without iron, Co:Si = 0.37:1 [39]. Taking into account the stoichiometry of the talc structure and the chemical analysis, the resulting catalyst is a composite material constituted of layered metal silicate hydroxide particles dispersed in an aerogel matrix. The amount of catalyst particles with respect to the aerogel is about 20% w/w.

Figure 1. X-ray diffraction (XRD) profiles of catalysts aer-CoFeSi (**a**) and aer-CoSi (**b**).
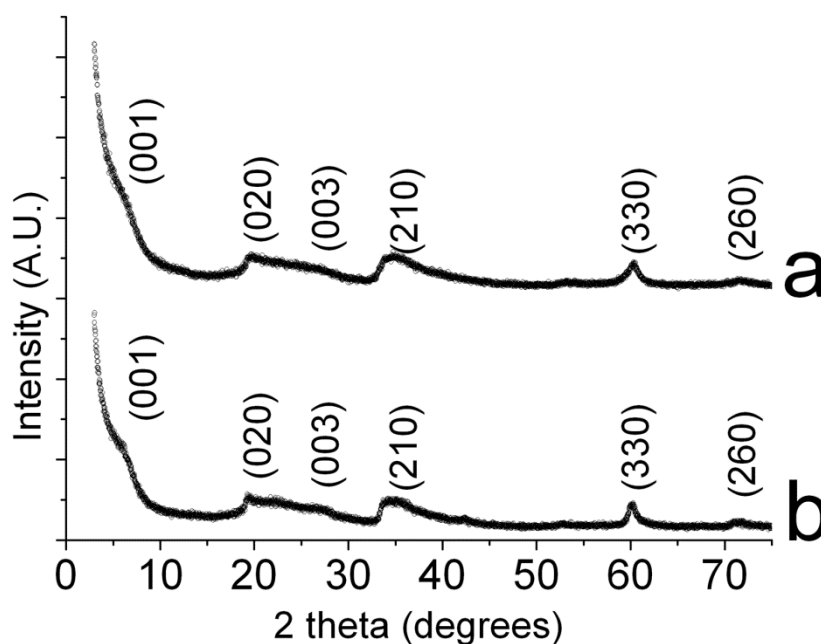
The characterization of the catalyst coatings onto the honeycomb structures was carried out by electron microscopy and X-ray photoelectron spectroscopy. Figure 2 shows a picture of the cordierite honeycomb before and after deposition of the *aer-CoFeSi* catalyst. Figure 3 shows scanning electron microscopy (SEM) images recorded over individual channels of *aer-CoFeSi* and *aer-CoSi* catalytic honeycombs as well as of a cordierite channel before deposition. An excellent deposition of the catalysts is achieved, covering all the surface of the channels, including the interior of the wall pores. At high magnification, the particles of the talc structure are clearly observed which, according to the XRD results, exhibit a well-defined layered morphology. For both samples the morphology of the talc layers is similar and measures about 1.5 μm × 300 nm × 50 nm. The catalytic particles are strongly anchored over the aerogel host. No weight loss is observed when the catalytic honeycombs are exposed to mechanical vibration stress tests up to 15 G and 100 Hz for 30 min (NTP conditions).

Figure 4 shows a SEM image corresponding to the *aer-CoFeSi* catalytic honeycomb recorded after a FIB cut perpendicular to the channel direction. In this way the thickness of the catalyst layer can be directly measured, which is about 8 μm. Interestingly, several pores of the honeycomb structure are also visible and are coated with catalyst as well. The layered structure of the cobalt talc structure doped with iron is clearly visible within the catalytic layer along with the classical cluster-of-grape morphology of SiO_2 aerogel. The X-ray maps corresponding to the area enclosed within the square for

Co, Fe, Si and Al (K_α signals) are depicted also in Figure 4. Clearly, Co and Fe signals are located within the catalyst layer, both at the channel's surface and at the interior of honeycomb pores, where the Co signal is more intense, as expected from the catalyst formulation. Contrarily, the Al signal is restricted to the cordierite substrate and the Si signal exhibits contribution both from the cordierite support (more intense) and the catalyst. The Fe/Co atomic ratio of the catalyst layer obtained by energy dispersive X-ray analysis (EDX) is about 0.12, very close to the bulk value determined by XRF.

Figure 2. Images of the honeycomb structures (400 cpsi) used in this work (**a**) and loaded with the *aer-CoFeSi* catalyst (**b**).
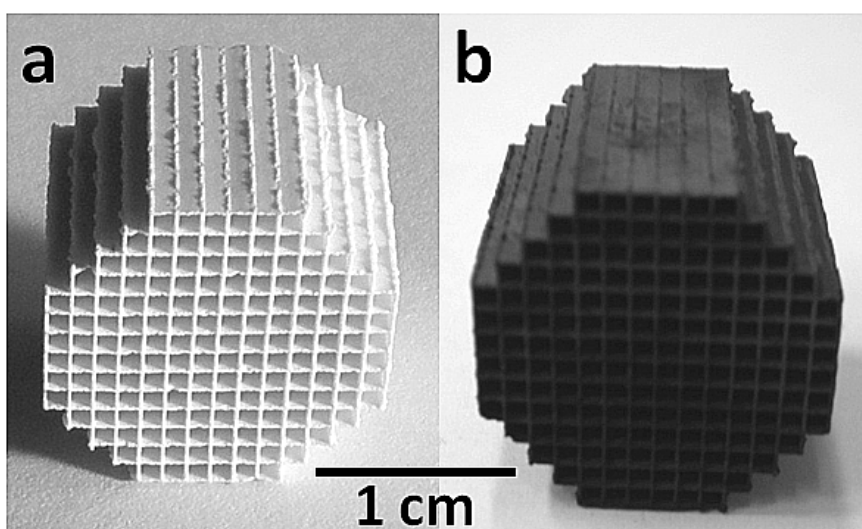

Figure 3. SEM images taken at several magnifications of the interior of a monolith channel (**a**,**b**) and loaded with *aer-CoFeSi* (**c**,**d**) and *aer-CoSi* (**e**,**f**) catalysts.
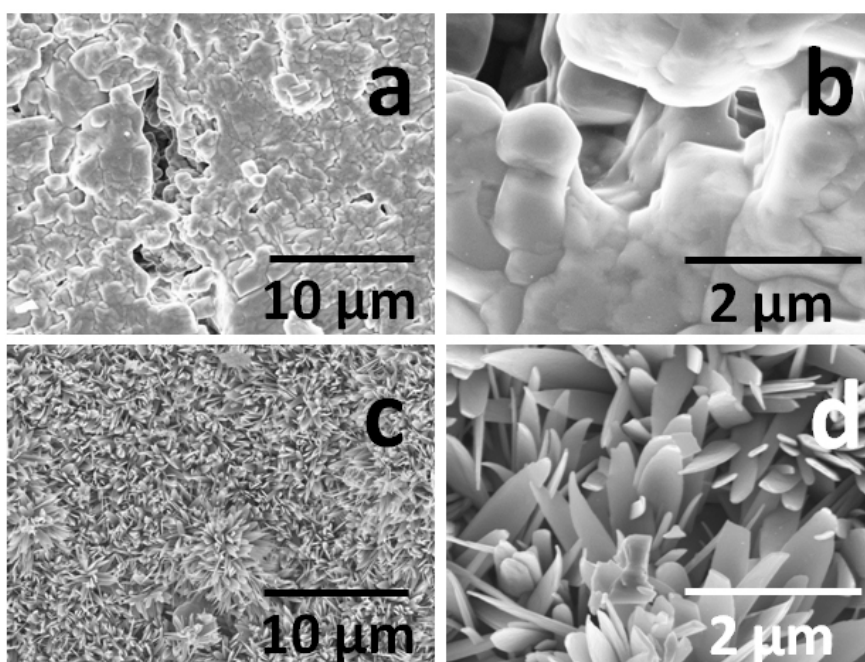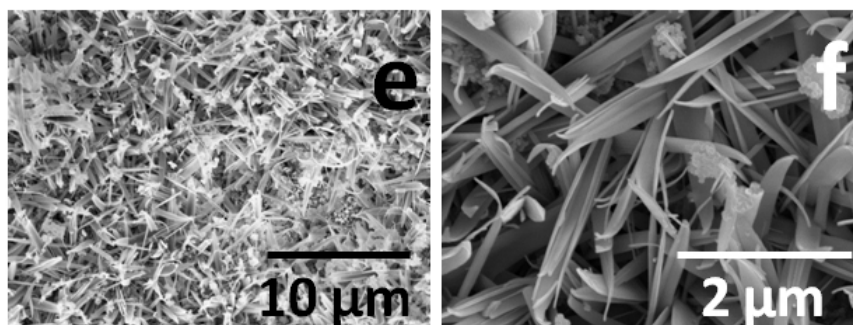
Figure 4. SEM image corresponding to the interior of a monolith channel loaded with *aer-CoFeSi* catalysts after a perpendicular focus ion beam (FIB) cut and X-ray maps recorded over the same area for Co, Fe, Si and Al (K_α lines).
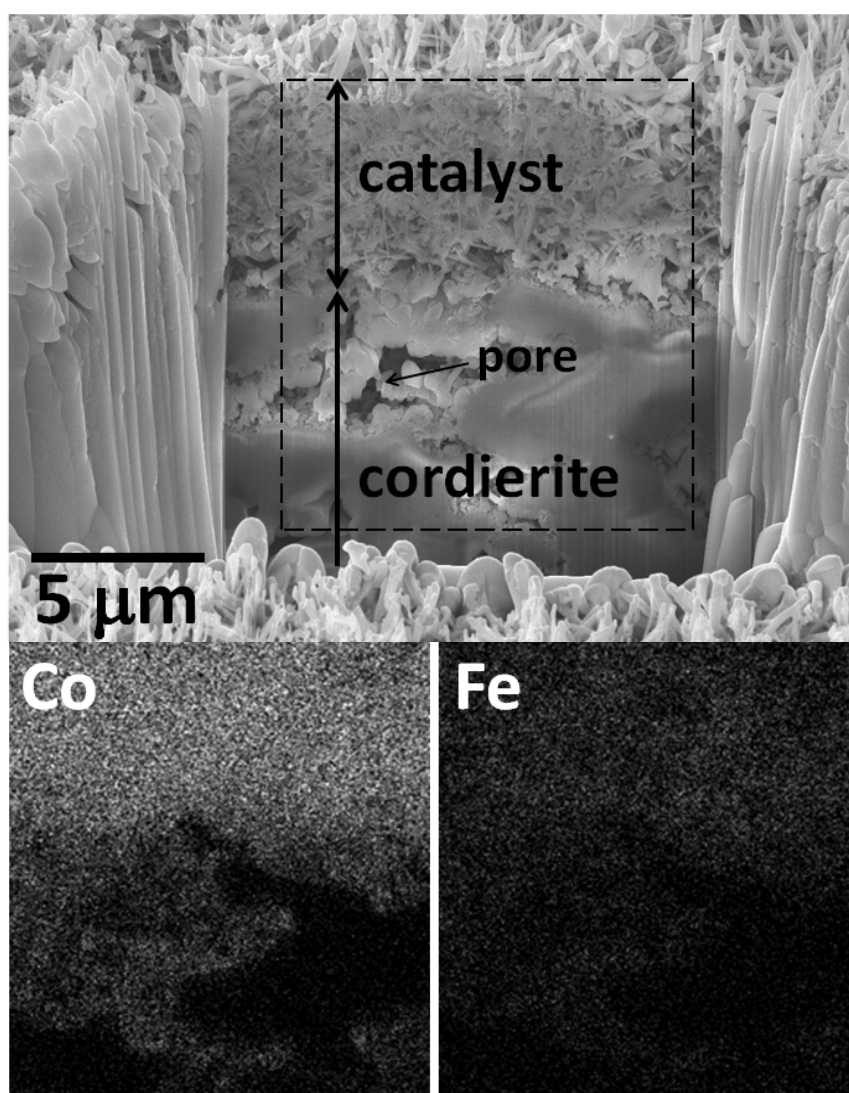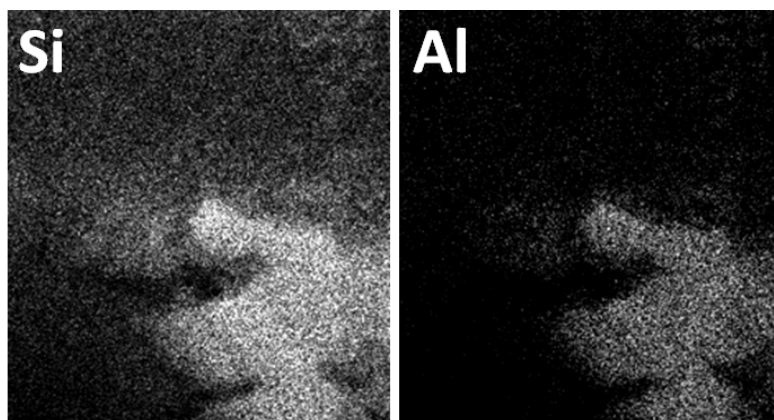
Figure 4. *Cont.*

Several channels were examined by X-ray photoelectron spectroscopy (XPS) to study the chemical homogeneity of the catalytic surface. Figure 5 shows a representative relative atomic concentration line scan along one channel of the *aer-CoFeSi* honeycomb. XPS line scan analyses reveal that $(Co,Fe)_3[Si_2O_5]_2(OH)_2$ is distributed along all the channel, as expected. However, the distribution is not completely homogeneous, as a higher amount of Co and Fe is found at the edges, while a higher content of Si and Al from silica aerogel and cordierite $(Mg_2Al_4Si_5O_{18})$ is observed at the center of the channels. This phenomenon could be generated during the free impregnation of the silica alcogel with the metal precursor salts and/or during supercritical drying. Interestingly, the atomic ratio Fe/Co is maintained at an approximately constant value. A surface segregation of Fe is observed (Fe/Co~0.6–0.7) with respect to the bulk value of Fe/Co = 0.13. In all cases, the Co $2p_{3/2}$ and Fe $2p_{3/2}$ binding energy values recorded (780.6 and 711 eV, respectively) correspond to both oxidized Co and Fe surface species.

Figure 5. Atomic concentration line scan along one channel of an *aer-CoFeSi* honeycomb determined by XPS.
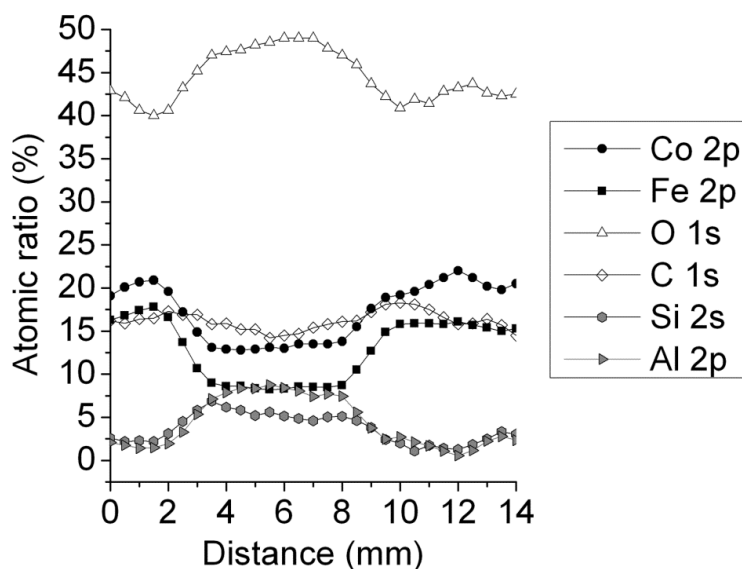
2.2. Catalytic Behavior

Ethanol conversion and selectivity values obtained over *aer-CoFeSi* and *aer-CoSi* catalytic honeycombs under low load of ethanol (diluted conditions) are reported in Table 1 at different temperatures. The *aer-CoSi* catalyst is more active for the ethanol steam reforming reaction than the *aer-CoFeSi* catalyst. Accordingly, the amount of acetaldehyde, which is an intermediate of the reaction (Equation 5), is higher in the case of the *aer-CoFeSi* sample compared to *aer-CoSi*. Also, the amount of dimethyl ketone is higher for *aer-CoFeSi* because it is formed by condensation of acetaldehyde [12]. For both catalytic honeycombs, as the temperature increases so does the amount of the reforming products, H_2 and CO_2, according to the endothermic character of the reaction. At 673 K ethanol conversion is total and there are no traces of acetaldehyde or dimethyl ketone among the reaction products for both catalysts. Under these conditions, the amount of hydrogen obtained is higher with the *aer-CoFeSi* sample, 72.8% *vs.* 70.7% for *aer-CoSi*, with the theoretical maximum value at 75% (Equation 1). This is due to a better WGS activity (Equation 3) and, more interestingly, to a lower selectivity towards CH_4. The promoting effect of Fe for the WGS reaction during the ethanol steam reforming has been shown to occur over Co/ZnO and Rh/Ca-Al$_2$O$_3$ catalysts doped with Fe [37,46]. Methane can only be reformed at high temperature, so for an ethanol steam reforming process operating at moderate temperature it is important to avoid it, since methane formation sharply decreases the hydrogen yield. It can be concluded that doping cobalt talc with Fe results in a certain loss of activity for ESR but, conversely, to an important enhancement of hydrogen selectivity due to methane suppression. No signs of deactivation were observed after 80 h on stream for both samples.

Table 1. Ethanol conversion and product distribution (dry basis) over aer-CoFeSi and aer-CoSi catalytic honeycombs under ethanol steam reforming (ESR) conditions at different temperature. S/C = 3, W/F = 10^4 g·min·molEtOH^{-1}, VHSV = 680 h^{-1}.

Catalyst	T/K	EtOH conv./%	Selectivity/%					
			H_2	CO_2	CO	CH_4	CH_3CHO	$(CH_3)_2CO$
aer-CoFeSi	573	86	49.7	3.1	3.4	3.2	40.6	-
	598	93	57.8	6.5	2.0	3.9	28.6	1.2
	623	99	69.8	14.5	1.1	5.8	7.1	1.7
	673	100	72.8	23.0	0.9	3.3	-	-
aer-CoSi	573	92	66.7	16.6	5.2	7.0	4.1	0.4
	598	99	68.7	23.0	0.9	7.1	0.2	0.1
	623	100	68.7	23.2	1.0	7.1	-	-
	673	100	70.7	22.7	1.9	4.7	-	-

The catalytic performance of the *aer-CoFeSi* catalytic honeycomb was studied in detail under high load of ethanol (undiluted conditions) at several temperature and pressure conditions. Operation under moderate pressure is advantageous for practical application since it allows for compact fuel processors [1]. However, from the thermodynamics point of view, an increase of reactor pressure is always unfavorable for steam reforming reactions [42]. Therefore, the study of the catalytic performance under various pressure values is important. Figure 6a shows the yields for the different products attained at 673 K over the *aer-CoFeSi* catalytic honeycomb by varying the pressure between 1

and 7 bar using a pure ethanol-water mixture with no diluents (S/C = 3) taking into account both the ethanol conversion and product selectivity. As the pressure is increased above 4 bar, the ethanol conversion decreases progressively, as expected, from about 85–87% down to 74%. Interestingly, the amount of acetaldehyde decreases when the pressure is increased (from 4.4% of selectivity on a dry basis at 1 bar down to 1.0% at 7 bar), suggesting that pressure affects less negatively the reforming of acetaldehyde (Equation 6) with respect to the dehydrogenation of ethanol into acetaldehyde (Equation 5), which is the first step of the reforming process over Co-based catalysts. Dimethyl ketone is kept constant at a selectivity value of ca. 0.3% for all pressure values. The decrease of ethanol transformation is accompanied by a significant decrease of hydrogen selectivity, whereas the amount of methane among the reaction products increases strongly with pressure, from 8% at 1 bar up to 18.4% at 7 bar. Methane formation is directly correlated with pressure, since reaction between carbon oxides and hydrogen to yield methane is progressively favored as pressure increases [42]. The effect of pressure is also observed for the WGS equilibrium; the higher the pressure the more carbon dioxide is obtained at the expense of CO. All these processes results in a different net amount of hydrogen generated; up to 3 bar the amount of hydrogen generated is kept approximately constant at about 1.6 $NL_{H2}\cdot s^{-1}$, whereas at pressures higher than 3 bar the production of hydrogen decreases progressively down to 1.0 $NL_{H2}\cdot s^{-1}$ at 7 bar. Figure 6b shows the product yield obtained at 7 bar by varying the temperature from 598 to 673 K. The reaction temperature has a strong effect on ethanol conversion at high pressure and, consequently, on hydrogen yield. At 7 bar, ethanol conversion drops from 74% at 673 K to 20% at 598 K, whereas the amount of acetaldehyde increases. The maximum hydrogen yield is obtained at 648–673 K. At 648 K the ethanol conversion is lower than at 673 K (66 *vs*. 74%), but the selectivity is better because an increase of reaction temperature results in a higher selectivity towards methane.

Figure 6. Ethanol conversion and product distribution (dry basis) over *aer-CoFeSi* catalytic honeycomb under ethanol steam reforming (ESR) conditions at 673 K and different pressure (**a**); and at 7 bar and different temperature (**b**). S/C = 3, W/F = 390 $g\cdot min\cdot mol_{EtOH}^{-1}$, volume hourly space velocity (VHSV) = 1800 h^{-1}. ▢ H_2, ▢ CO_2, ▉ CO, ■ CH_4, ▨ CH_3CHO.
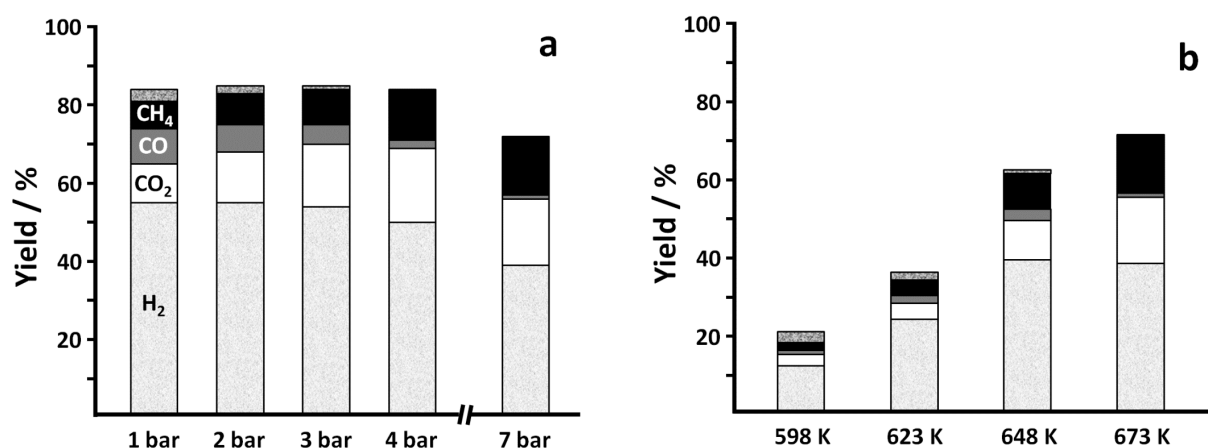
3. Experimental Section

3.1. Preparation of Catalysts

Cordierite monoliths (Corning, 400 cpsi) were used as a catalyst support. They were cut with a diamond saw with a cylindrical shape (18 mm diameter, 20 mm length, 156 cells). $Co_3[Si_2O_5]_2(OH)_2$ (cobalt talc) doped with Fe (Fe/Co = 0.1 molar ratio) in SiO_2 aerogel was grown over the cordierite honeycombs by a sol-gel method followed by supercritical drying [39]. First, the cordierite pieces were coated with a thin layer of silica alcogel through the hydrolysis and condensation of tetraethoxysilane (TEOS, $Si(OCH_2CH_3)_4$, 98% Sigma Aldrich) dissolved in ethanol. Gelation was catalyzed by addition of an aqueous solution of HNO_3 and HF (TEOS:EtOH:H_2O:HNO_3:HF = 1.0:6.0:15.9:0.03:0.12 molar ratio). Next, the alcogel was impregnated with an ethanolic solution containing both cobalt nitrate hexahydrate ($Co(NO_3)_2·6H_2O$, 99% Scharlau) and iron nitrate hexahydrate ($Fe(NO_3)_3·6H_2O$, 99% Scharlau) over 72 h. Finally, the solvent was extracted under supercritical conditions at 6.28×10^6 Pa and 516 K, which resulted in the formation of a thin layer of silica aerogel with cobalt talc doped with Fe over the cordierite surface. This is referred to in this work as *aer-CoFeSi*. Following exactly the same procedure, catalytic monoliths with cobalt talc were prepared in the absence of iron for comparative purposes, which are referred to as *aer-CoSi*. Powdered catalysts were obtained in the same reactor batches and used for characterization.

3.2. Characterization Techniques

Elemental composition of the powdered catalysts was determined by X-ray fluorescence (XRF) with a Phillips PW2400 apparatus. X-ray diffraction (XRD) measurements were performed with a Siemens D5000X diffractometer equipped with a Cu K_α X-ray source. XRD analyses were performed in the 2θ range of 3 to 75° at a stepsize of 0.02°. A Micromeritics ASAP 2000 apparatus was used to study the Brunauer-Emmet-Teller (BET) surface area and Barret-Joyner-Halenda (BJH) pore size of the powdered catalysts. A Zeiss Neon 40 focused ion beam electron microscope with cross beam (FIB-SEM) and energy-dispersive X-ray detector (EDX) was used in order to study directly the microstructure and element distribution of the catalytic layers in the honeycomb structures. X-ray photoelectron spectroscopy (XPS) was performed using a Kratos AXIS Ultra DLD spectrometer and a monochromatic X-ray source (Al K_α). An automatic charge neutralizer system was used. Binding energy values were calibrated at 285.0 eV corresponding to the adventitious C1s reference.

3.3. Reaction Tests

The catalytic honeycombs were tested in a tubular stainless steel reactor. Prior to catalytic tests the samples were heated up to 473 K in air for 20 min. The effect of reaction temperature was first studied at atmospheric pressure under diluted conditions with a mixture of EtOH:H_2O:N_2 = 1:3:96 molar (S/C = 1.5), W/F = 10^4 g·min·mol$_{EtOH}^{-1}$, VHSV = 680 h^{-1}. The catalysts were exposed to the reaction mixture at 573, 598, 623, and 673 K over 80 h to check for deactivation. The same samples were then studied under high loads of ethanol and water at S/C = 3 with no carrier gas in order to simulate real conditions. The liquid mixture of reactants was supplied directly into the reactor with a Knauer

Smartline HPLC pump (0.075 mL·min^{-1}). The performance of the catalytic honeycombs was studied between 598 and 673 K and between 1 and 7 bar under W/F = 390 g·min·mol$_{EtOH}$$^{-1}$, VHSV = 1800 h^{-1}. The reactor effluent was analyzed on line by gas chromatography using an Agilent 3000A apparatus equipped with MS 5Å, PlotU and Stabilwax columns. Conversion and selectivity values are defined as follows (Equations 8 and 9):

$$\text{EtOH conversion (\%)} = 100 \ (n_{EtOH\ conv}/2\ n_{EtOH\ in}) \tag{8}$$

$$\text{Selectivity to C}_i \text{ species (\%)} = 100 \ (n_{Ci}/\Sigma n_{Ci}) \tag{9}$$

where $n_{EtOH\ conv}$ represents the moles of ethanol converted, measured as the sum of moles of CO_2, CO, CH_4, CH_3CHO and $(CH_3)_2CO$ at the reactor outlet and $n_{EtOH\ in}$ represents the moles of ethanol at the reactor inlet.

4. Conclusions

Honeycomb structures have been loaded with catalysts containing cobalt talc ($Co_3[Si_2O_5]_2(OH)_2$) doped with Fe (Fe/Co~0.1) in a SiO_2 aerogel host. The catalytic composite has been prepared directly over cordierite honeycomb pieces from silica alcogel impregnated with metal nitrates by supercritical drying. In addition, to favor mass transfer characteristics, the silica aerogel host allows an excellent dispersion of catalyst particles, which remain well adhered during reaction. The honeycomb catalyst has been tested in the ethanol steam reforming reaction aimed at producing hydrogen for on-board, on-demand applications at moderate temperature (573–673 K) and pressure (1–7 bar). Compared to non-promoted cobalt talc, the catalyst doped with iron is less active but produces less methane as byproduct, resulting in higher hydrogen yields. At 673 K and up to 3 bar, the amount of hydrogen generated is kept approximately constant at about 1.6 $NL_{H2}\cdot s^{-1}$ under S/C = 3 and W/F = 390 g·min·mol$_{EtOH}$$^{-1}$.

Conflict of Interest

The authors declare no conflict of interest.

References

1. Kolb, G. *Fuel Processing for Fuel Cells*; Wiley-VCH: Weinheim, Germany, 2008; pp. 1-434.
2. Llorca, J. Microreactors for the Generation of Hydrogen from Ethanol. In *Handbook of Sustainable Energy*; Lee, W.H., Cho, V.G., Eds.; Nova Publishers: New York, NY, USA, 2010; pp. 693–699.

3. Murdoch, M.; Waterhouse, G.I.N.; Nadeem, M.A.; Metson, J.B.; Keane, M.A.; Howe, R.F.; Llorca, J.; Idriss, H. The effect of gold loading and particle size on photocatalytic hydrogen production from ethanol over Au/TiO$_2$ nanoparticles. *Nat. Chem.* **2011**, *3*, 489–492.

4. Vaidya, P.D.; Rodrigues, A.E. Insight into steam reforming of ethanol to produce hydrogen for fuel cells. *Chem. Eng. J.* **2006**, *117*, 39–49.

5. Haryanto, A.; Fernando, S.; Murali, N.; Adhikari, S. Current status of hydrogen production techniques by steam reforming of ethanol: A review. *Energy Fuels* **2005**, *19*, 2098–2106.

6. Ni, M.; Leung, Y.C.; Leung, M.K.H. A review on reforming bio-ethanol for hydrogen production. *Int. J. Hydrog. Energy* **2007**, *32*, 3238–3247.

7. Deluga, G.A.; Salge, J.R.; Schmidt, L.D.; Verykios, X.E. Renewable hydrogen form Ethanol by autothermal reforming. *Science* **2004**, *303*, 993–997.

8. Frusteri, F.; Freni, S. Bio-ethanol, a suitable fuel to produce hydrogen for a molten carbonate fuel cell. *J. Power Sources* **2007**, *173*, 200–209.

9. Idriss, H.; Scott, M.; Llorca, J.; Chan, S.C.; Chiu, W.; Sheng, P.Y.; Yee, A.; Blackford, M.A.; Pas, S.J.; Hill, A.J.; *et al*. A phenomenological study of the metal-oxide interface: The role of catalysis in hydrogen production from renewable resources. *ChemSusChem* **2008**, *1*, 905–910.

10. Haga, F.; Nakajima, T.; Miya, H.; Mishima, S. Catalytic properties of supported cobalt catalysts for steam reforming of ethanol. *Catal. Lett.* **1997**, *48*, 223–227.

11. Llorca, J.; Homs, N.; Sales, J.; de la Piscina, P.R. Efficient production of hydrogen over supported cobalt catalysts from ethanol steam reforming. *J. Catal.* **2002**, *209*, 306–317.

12. Llorca, J.; de la Piscina, P.R.; Dalmon, J.A.; Sales, J.; Homs, N. CO-free hydrogen from steam-reforming of bioethanol over ZnO-supported cobalt catalysts: Effect of metallic precursor. *Appl. Catal. B* **2003**, *43*, 355–369.

13. Llorca, J.; Dalmon, J.A.; de la Piscina, P.R.; Homs, N. *In situ* magnetic characterisation of supported cobalt catalysts under steam-reforming of ethanol. *Appl. Catal. A* **2003**, *243*, 261–269.

14. Freni, S.; Cavallaro, S.; Mondello, N.; Spadaro, L.; Frustreri, F. Production of hydrogen for MC fuel cell by steam reforming of ethanol over MgO supported Ni and Co catalysts. *Catal. Commun.* **2003**, *4*, 259–268.

15. Mariño, F.; Baronetti, G.; Jobbagy, M.; Laborde, M. Cu-Ni-K/γ-Al$_2$O$_3$ supported catalysts for ethanol steam reforming: Formation of hydrotalcite-type compounds as a result of metal-support interaction. *Appl. Catal. A* **2003**, *238*, 41–54.

16. Llorca, J.; Homs, N.; Sales, J.; Fierro, J.L.G.; de la Piscina, P.R. Effect of sodium addition on the performance of Co-ZnO-based catalysts for hydrogen production from bioethanol. *J. Catal.* **2004**, *222*, 470–480.

17. Llorca, J.; de la Piscina, P.R.; Dalmon, J.A.; Homs, N. Transformation of Co$_3$O$_4$ during ethanol steam-re-forming. Activation process for hydrogen production. *Chem. Mater.* **2004**, *16*, 3573–3578.

18. Llorca, J.; Homs, N.; de la Piscina, P.R. *In situ* DRIFT-mass spectrometry study of the ethanol steam-reforming reaction over carbonyl-derived Co/ZnO catalysts. *J. Catal.* **2004**, *227*, 556–560.

19. Batista, M.S.; Santos, R.K.S.; Assaf, E.M.; Assaf, J.M.; Ticianelli, E.A. High efficiency steam reforming of ethanol by cobalt-based catalysts. *J. Power Sources* **2004**, *134*, 27–32.

20. Kaddouri, A.; Mazzocchia, C. A study of the influence of the synthesis conditions upon the catalytic properties of Co/SiO$_2$ or Co/Al$_2$O$_3$ catalysts used for ethanol steam reforming. *Catal. Commun.* **2004**, *5*, 339–345.

21. Song, H.; Zhang, L.; Watson, R.B.; Braden, D.; Ozkan, U. Investigation of bio-ethanol steam reforming over cobalt-based catalysts. *Catal. Today* **2007**, *129*, 346–354.

22. Torres, J.A.; Llorca, J.; Casanovas, A.; Domínguez, M.; Salvadó, J.; Montané, D. Steam reforming of ethanol at moderate temperature: Multifactorial design analysis of Ni/La$_2$O$_3$-Al$_2$O$_3$, and Fe- and Mn-promoted Co/ZnO catalysts. *J. Power Sources* **2007**, *169*, 158–166.

23. Benito, M.; Padilla, R.; Rodríguez, L.; Sanz, J.L.; Daza, L. Zirconia supported catalysts for bioethanol steam reforming: Effect of active phase and zirconia structure. *J. Power Sources* **2007**, *169*, 167–176.

24. Tutti, S.; Pepe, F. On the catalytic activity of cobalt oxide for steam reforming of ethanol. *Catal. Lett.* **2008**, *122*, 196–203.

25. Song, H.; Ozkan, U. Ethanol steam reforming over Co-based catalysts: Role of oxygen mobility. *J. Catal.* **2009**, *261*, 66–74.

26. Casanovas, A.; de Leitenburg, C.; Trovarelli, A.; Llorca, J. Catalytic monoliths for ethanol steam reforming. *Catal. Today* **2008**, *138*, 187–192.

27. Casanovas, A.; Saint-Gerons, M.; Griffon, F.; Llorca, J. Autothermal generation of hydrogen from ethanol in a microreactor. *Int. J. Hydrog. Energy* **2008**, *33*, 1827–1833.

28. Llorca, J.; Casanovas, A.; Trifonov, T.; Rodríguez, A.; Alcubilla, R. First use of macroporous silicon loaded with catalyst film for a chemical reaction: A microreformer for producing hydrogen from ethanol steam reforming. *J. Catal.* **2008**, *255*, 228–233.

29. Wang, H.; Ye, J.L.; Liu, Y.; Li, Y.D.; Qin, Y.N. Steam reforming of ethanol over Co$_3$O$_4$/CeO$_2$ catalysts prepared by different methods. *Catal. Today* **2007**, *129*, 305–312.

30. Sun, J.; Qiu, X.-P.; Wu, F.; Zhu, W.-T. H$_2$ from steam reforming of ethanol at low temperature over Ni/Y$_2$O$_3$, Ni/La$_2$O$_3$ and Ni/Al$_2$O$_3$ catalysts for fuel-cell applications. *Int. J. Hydrog. Energy* **2005**, *30*, 437–445.

31. Galetti, A.E.; Gomez, M.F.; Arrua, L.A.; Marchi, A.J.; Abello, M.C. Study of CuCoZnAl oxide as catalyst for the hydrogen production from ethanol reforming. *Catal. Commun.* **2008**, *9*, 1201–1208.

32. Vargas, J.C.; Libs, S.; Roger, A.C.; Kiennemann, A. Study of Ce-Zr-Co fluorite-type oxide as catalysts for hydrogen production by steam reforming of bioethanol. *Catal. Today* **2005**, *107*, 417–425.

33. Casanovas, A.; Domínguez, M.; Ledesma, C.; López, E.; Llorca, J. Catalytic walls and micro-devices for generating hydrogen by low temperature steam reforming of ethanol. *Catal. Today* **2009**, *143*, 32–37.

34. Nedyalkova, R.; Casanovas, A.; Llorca, J.; Montané, D. Electrophoretic deposition of Co-Me/ZnO (Me = Mn, Fe) ethanol steam reforming catalysts on stainless steel plates. *Int. J. Hydrog. Energy* **2009**, *34*, 2591–2599.

35. Casanovas, A.; de Leitenburg, C.; Trovarelli, A.; Llorca, J. Ethanol steam reforming and water gas shift reacion over Co-Mn/ZnO catalysts. *Chem. Eng. J.* **2009**, *154*, 267–273.

36. López, E.; Irigoyen, A.; Trifonov, T.; Rodríguez, A.; Llorca, J. A milion-channel reformer on a fingertip: Moving down the scale in hydrogen production. *Int. J. Hydrog. Energy* **2010**, *35*, 3472–3479.

37. Casanovas, A.; Roig, M.; de Leitenburg, C.; Trovarelli, A.; Llorca, J. Ethanol steam reforming and water gas shift over Co/ZnO catalytic honeycombs doped with Fe, Ni, Cu, Cr and Na. *Int. J. Hydrog. Energy* **2010**, *35*, 7690–7698.

38. Bichon, P.; Haugom, G.; Venvik, H.J.; Colmen, A.E.; Blekkan, A. Steam reforming of ethanol over supported Co and Ni catalysts. *Top. Catal.* **2008**, *49*, 38–45.

39. Domínguez, M.; Taboada, E.; Molins, E.; Llorca, J. Co-SiO_2 aerogel-coated catalytic walls for the generation of hydrogen. *Catal. Today* **2008**, *138*, 193–197.

40. Domínguez, M.; Cristiano, G.; López, E.; Llorca, J. Ethanol steam reforming over cobalt talc in a plate microreactor. *Chem. Eng. J.* **2011**, *176–177*, 280–285.

41. Domínguez, M.; Taboada, E.; Idriss, H.; Molins, E.; Llorca, J. Fast and efficient hydrogen generation catalyzed by cobalt talc nanolayers dispersed in silica aerogel. *J. Mater. Chem.* **2010**, *20*, 4875–4883.

42. Domínguez, M.; Taboada, E.; Molins, E.; Llorca, J. Ethanol steam reforming at very low temperature over cobalt talc in a membrane reactor. *Catal. Today* **2012**, doi:10.1016/j.cattod.2012.02.004.

43. Sekine, Y.; Kazama, A.; Izutsu, Y.; Matsukata, M.; Kikuchi, E. Steam reforming of ethanol over cobalt catalysts modified with a small amount of iron. *Catal. Lett.* **2009**, *132*, 329–334.

44. Kazama, A.; Sekine, Y.; Oyama, K.; Matsukata, M.; Kikuchi, E. Promoting effect of small amount of Fe addition onto Co catalyst supported on α-Al_2O_3 for steam reforming of ethanol. *Appl. Catal. A* **2010**, *383*, 96–101.

45. Zhang, G.; Zhao, Y.; Tao, F.; Li, H.J. Electrochemical characteristics and impedance spectroscopy studies of nano-cobalt silicate hydroxide for supercapacitor. *J. Power Sources* **2006**, *161*, 723–729.

46. Chen, L.; Kai, C.; Zhong, Z.; Huang, L.; Peng, T.; Hong, L.; Lin, J. Carbon monoxide-free hydrogen production via low-temperature steam reforming of ethanol over iron-promoted Rh catalyst. *J. Catal.* **2010**, *276*, 197–200.